Interlocking-induced stiffness in stochastically microcracked materials beyond the transport percolation threshold

R. C. Picu,[1,*] A. Pal,[1] and M. V. Lupulescu[2]

[1]*Department of Mechanical, Aerospace and Nuclear Engineering, Rensselaer Polytechnic Institute, Troy, New York 12180, USA*
[2]*New York State Museum, Research and Collections, 3140 CEC, Albany, New York 12230, USA*

We study the mechanical behavior of two-dimensional, stochastically microcracked continua in the range of crack densities close to, and above, the transport percolation threshold. We show that these materials retain stiffness up to crack densities much larger than the transport percolation threshold due to topological interlocking of sample subdomains. Even with a linear constitutive law for the continuum, the mechanical behavior becomes nonlinear in the range of crack densities bounded by the transport and stiffness percolation thresholds. The effect is due to the fractal nature of the fragmentation process and is not linked to the roughness of individual cracks.

I. INTRODUCTION

Most materials in use today contain randomly distributed microcracks or pores which are introduced by overloads or are due to the presence of weak interfaces such as grain boundaries. If the crack density is small, the sample modulus is close to the modulus of the virgin material and methods to predict the softening effect of such distributed damage exist (e.g., [1]). As the crack density increases, the transport percolation threshold, P_t, is reached and a continuous path linking microcracks across the sample can be found. P_t has been found using lattice and continuum models, in two dimensions (2D) [2,3] and three dimensions (3D) [4]. It is generally believed that 3D samples preserve stiffness at crack densities above the transport percolation limit; however, in the 2D case the transport and stiffness percolation thresholds coincide and hence samples with crack densities above P_t cannot carry loads [5,6]. Here we revisit this concept and show that, even in the 2D case, stiffness percolation is reached at crack densities significantly larger than those corresponding to P_t, and that this is due to the topological interlocking of sample subdomains resulting during the fragmentation process. We refer to stiffness percolation as the threshold below which the sample carries loads at infinitesimal or finite strains.

Topological interlocking represents a potential avenue towards a conceptually different class of materials whose behavior is dominated by the large number of internal nonbonded interfaces. The concept has been studied recently in the context of material design [7–10]. In these works, bodies are assembled from identical parts whose shape is designed such to allow interlocking. The integrity of the resulting object is insured by the shape of the constituent elements or/and by a confining pressure applied along the boundaries. These structures are interesting due to a number of reasons: (a) in case of damage, cracks are trapped at interfaces between components [11], (b) penetration of projectiles leaves only localized damage [12], (c) such structures have interesting vibration-absorbing properties [13], etc.

Interlocking occurs in living and nonliving natural materials leading to increased toughness. An example is the interaction of mineralized collagen regions in turtle shells [8]. In brittle materials, such as bone, a toughening mechanism is crack bridging by ligaments left behind the crack front, which are connected to the two crack faces by well-bonded interfaces or by interlocking [14]. Also, nanoscale interlocked materials have been created by the self-assembly of octopod-shaped nanocrystals into 3D porous superlattices [15]. A particularly interesting example in which interlocking dominates the mechanical behavior is that of itacolumite, known also as the "flexible sandstone" [16,17]. This rock is composed from quartz grains grouped in well-bonded small clusters. The clusters are separated by gaps of approximately 1 μm width. The rock exhibits spectacular flexibility, with plates of 2–3 cm thickness and several tens of cm length having deflections on the order of several cm when loaded in bending with small forces [17]; see Supplemental Material [18]. This behavior has inspired the development of flexible man-made ceramics [19,20], which, however, are not used broadly due to their reduced strength and stiffness relative to the corresponding monolithic ceramics.

In a polycrystal which fractures along grain boundaries, interlocking of the two crack faces may result if the grains are very irregular in shape or if the grain boundaries are rough. In this work we show that these features are not required to produce interlocking. We also emphasize that constructing materials with periodic microstructures such as in [7,9,10,13] is inefficient and that topologically interlocked materials with stochastic microstructure can be easily manufactured by bringing the system close to, but above, the critical point of transport percolation.

We focus on the 2D problem for which it is generally considered that the transport and stiffness percolation thresholds coincide [5,6]. Besides the theoretical interest, the 2D version of the problem represents brittle films, and layered quasi-2D structures such as the sedimentary rock itacolumite and most artificial interlocked materials described above.

II. MODEL AND SIMULATION PROCEDURE

To study the interlocking problem we consider structures with stochastic microstructure such as that shown in Fig. 1. The geometry is constructed in two steps. First, a set of grains
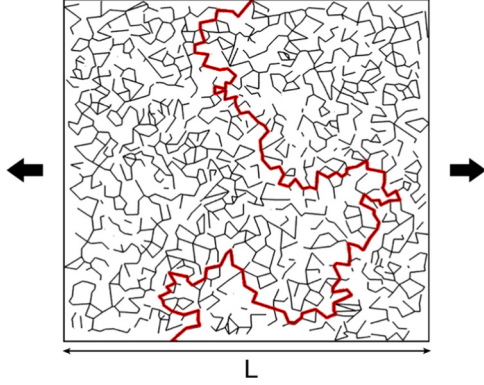
*Corresponding author: picuc@rpi.edu

FIG. 1. Crack pattern in a model with $f = 0.67$ fraction of cracked boundaries. The cracked boundaries are shown in black and the uncracked boundaries are not shown. This model contains a single percolated path (red thick line).

(not shown in Fig. 1) is defined using a Voronoi tessellation of the square problem domain of size L. The grains are equiaxed and of mean size, $\bar{d}$. The grain boundaries are straight lines. In the second step, cracks are introduced at random at a fraction f of the grain boundaries. Each crack spans the entire grain boundary and may connect with a neighboring crack at grain triple junctions. All grains are made from the same isotropic and linear elastic material of Young's modulus E_0 and Poisson ratio ν_0.

The model is loaded in uniaxial tension by applying imposed displacements on the right and left faces, while keeping the top and bottom faces traction free. The effective modulus of the sample, E_{eff}, is computed based on the resulting tractions and the imposed global strain. The solution is obtained by discretizing the structure into finite elements. The cracks are represented using surface interactions (contact and cohesive elements) which act in opening, overclosure, and shear. The opening and shear stiffness is $10^{-4}E_0$, while the overclosure stiffness is equal to E_0 and acts once the over-closure displacement is larger than $10^{-5}L$ (or $3.2 \times 10^{-4}\ \bar{d}$). We consider models containing $10^3, 10^4, 10^5$, and 10^6 grains ($L = 31.6\bar{d}$, $10^2\bar{d}$, $316.2\bar{d}$, $10^3\bar{d}$, respectively).

III. RESULTS AND DISCUSSION

A. Modeling results

Transport percolation occurs at a fraction of fractured boundaries, $f_{c1} = 0.667$ [2,3] (bond percolation threshold on 2D Voronoi lattices). In models of finite size, the percolation transition is not sharp. To mitigate the finite size effect, we generate a large number of structures for each f and $L/\bar{d}$ and, for $f > f_{c1}$, retain only structures in which at least one percolated path is found. To identify such structures, the crack geometry is treated as a graph and the largest connected component (in terms of vertical span) is determined. The largest span is the same as the vertical span of the largest cluster of connected bonds, which is what is used in the Hoshen-Kopelman algorithm. If the largest span is suitably close to L, the structure is considered percolated.

The structures with $f > f_{c1}$ are characterized using a geometric measure, m, indicating the likelihood to encounter
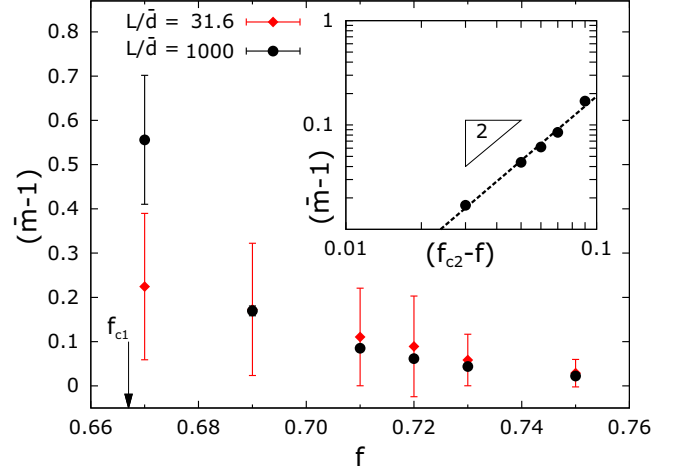

FIG. 2. Variation of the measure of overhangs, $\bar{m} - 1$, with f, for $f > f_{c1}$ and for two model sizes, $L/\bar{d} = 31.6$ and 10^3. The inset shows that $\bar{m} - 1 \sim (f_{c2} - f)^2$ in the vicinity of f_{c2}. Bars represent standard deviation based on 100 replicas and, for $L/\bar{d} = 10^3$ and $f \geqslant 0.69$, are of the size of the symbols.

overhangs on a percolated path. m is computed for the "shortest" percolated path of a structure with $f > f_{c1}$ as follows: (i) a weight is defined for each line segment (or grain boundary) via its vertically projected length, converting the crack structure into a undirected, weighted graph; (ii) nodes close to the top and bottom surfaces are collapsed into two nodes, respectively; (iii) the shortest path between the top node and bottom node is computed using Dijkstra's algorithm, and the length of this path is assigned to m. If the path has no overhangs preventing the free relative motion of the two parts of the sample, $m = L$, while $m > 1$ indicates the presence of overhangs. $\bar{m} - 1 = m/L - 1$ represents the fraction of grains forming overhangs, out of all the $L/\bar{d}$ grains aligned along the vertical edge of the model.

We study first the geometry of the structure described by $\bar{m} - 1$ which, as discussed below, is directly relevant to the body preserving stiffness for $f > f_{c1}$. Figure 2 shows the variation of $\bar{m} - 1$ with f for $f > f_{c1}$ and for two models with $L/\bar{d} = 31.6$ and 10^3. For f close to the transport percolation critical point f_{c1} (at $f = 0.67$), $\bar{m} - 1$ increases as the model size increases: $\bar{m} - 1 \sim (L/\bar{d})^{1.2}$. This is associated with the roughness of the percolation path which is characterized by a fractal dimension $D = 1.14$ (evaluated using the box counting method). This fractal dimension agrees with the value reported in the literature [21]. For larger f values the effect of the model size on $\bar{m} - 1$ is not observable within the accuracy of the present data set. In this regime, $\bar{m} - 1$ is only a function of f and vanishes at $f = f_{c2}$. The inset to Fig. 2 shows the variation of $\bar{m} - 1$ obtained with the largest model considered ($L/\bar{d} = 10^3$) with ($f_{c2} - f$), where the value of f_{c2} used, $f_{c2} = 0.78$, results by fitting the function $\bar{m} - 1 \sim (f_{c2} - f)^\alpha$ to the data. This power law variation is an adequate representation of the data for $f \geqslant 0.69$ and the exponent is $\alpha = 2.0 \pm 0.1$.

The effective stiffness of samples with a broad range of f values was evaluated numerically and the results are reported in Fig. 3. As f increases from zero ($f < f_{c1}$), only small modulus variations are observed. This regime was extensively
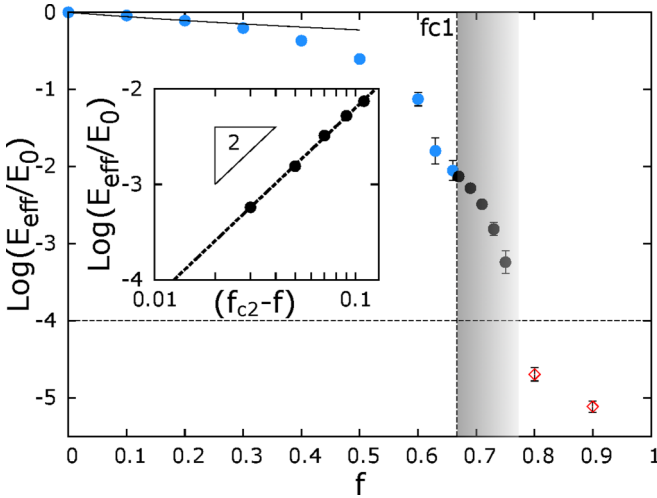
FIG. 3. Variation of the normalized effective stiffness with f. The vertical dashed line indicates the transport percolation threshold, f_{c_1}. The horizontal dashed line indicates the largest stiffness of a model with at least one percolated path with no interlocking. The continuous line shows the prediction of the model in [24] valid in the limit $f \to 0$. The shade indicated the range of f in which interlocking controls the mechanical behavior. The shape and color of symbols indicates the three regimes: nonpercolated (blue circles), percolated with interlocking (black filled circles), and percolated without interlocking (red open diamonds). The inset shows the power law variation of the effective stiffness in the vicinity of $f_{c_2} = 0.78$. All data obtained with model with $L/\bar{d} = 10^3$.

studied and several mean field theories exist for the low f end of the curve (e.g., [22,23]). The line represents the prediction of the theory developed in [24] based on the assumption of weak interaction of microcracks, $E_{\text{eff}}/E_0 = 1/(1 + \pi f)$. The mean field model works reasonably well up to large f values (e.g., [25]). The behavior close to, but below, the critical point ($f \lesssim f_{c_1}$) was also studied and it is reported that in this regime $E_{\text{eff}} \sim (f_{c_1} - f)^{\tau_E}$. Different models predict different exponents τ_E (e.g., 4.67 [6], 6.67 [26]). This critical point formulation obviously implies that the stiffness vanishes at the transport percolation threshold. The data in Fig. 3 (obtained with the model with $L/\bar{d} = 10^3$) indicate the opposite: *Samples preserve stiffness at f much larger than f_{c_1}.* Let us reemphasize that, in order to eliminate the finite size effect in the vicinity of f_{c_1}, all data points for $f > f_{c_1}$ (right of the vertical line in Fig. 3) correspond to samples containing at least one percolated path. The horizontal line in Fig. 3 corresponds to the stiffness expected for a sample with a percolated path with no overhangs. This limit results from the stiffness of the opening mode of the interface elements modeling the cracks and is the largest stiffness that can be obtained for percolated structures with no overhangs. Smaller values result if multiple percolated paths are present. The inset to Fig. 3 shows that in the vicinity of f_{c_2} the effective stiffness can be approximated as $E_{\text{eff}}/E_0 \sim (f_{c_2} - f)^{\beta}$, where $\beta = 2.0 \pm 0.1$. Data obtained with the model with $L/\bar{d} = 10^3$ are used in the inset and $f_{c_2} = 0.78$ results from fitting.

This discussion indicates the existence of a stiffness percolation threshold, f_{c_2}, with f_{c_2} significantly larger than f_{c_1}. The observation that $f_{c_2} > f_{c_1}$ in 2D is the main result of
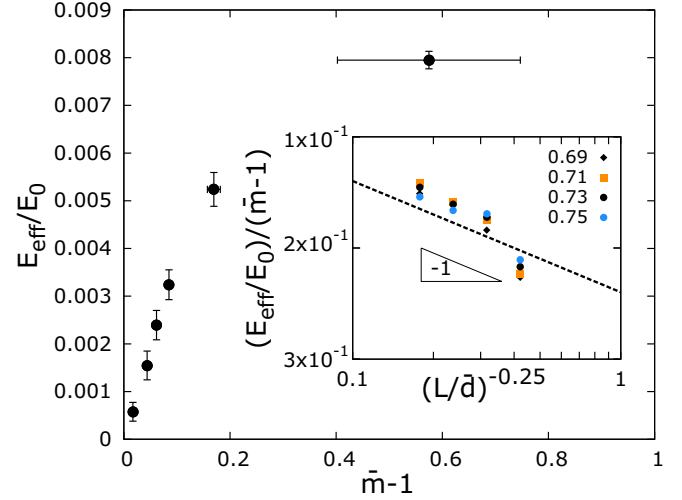

FIG. 4. Variation of the normalized effective stiffness with the geometric parameter $\bar{m} - 1$ indicating the presence of overhangs and hence interlocking. The inset shows the variation of function g defined in text with the model size, with different symbols indicating different f values. The line of slope–1 was added to guide the eye.

this article. This result is known in 3D [27], but the stiffness percolation threshold is not available [28].

The relation between E_{eff}/E_0 and $\bar{m} - 1$ is shown in Fig. 4 for the model with $L/\bar{d} = 10^3$; the two quantities are proportional for $f \to f_{c_2}$. However, E_{eff}/E_0 is more sensitive to the size of the model than $\bar{m} - 1$. As the model size increases, E_{eff}/E_0 increases for all $f > f_{c_1}$ and one can write $E_{\text{eff}}/E_0 = (\bar{m} - 1)_{(f)} g(L/\bar{d})$ for $f_{c_1} < f < f_{c_2}$. The inset to Fig. 4 shows function g for four values of $f = 0.69, 0.71, 0.73$, and 0.75 and for $L/\bar{d}$ from 31.6 to 10^3. For $L/\bar{d} > 31.6$ the data collapse on a line of slope–1 indicating $g \sim (L/\bar{d})^{\gamma}$ with $\gamma = 0.25$.

It is necessary to put the present discussion in the perspective of the literature on transport vs stiffness percolation in networks and network-based representations of continua. A significant body of literature is dedicated to the question of whether the two thresholds are identical or not (in 2D and 3D) for various types of networks and fiber-to-fiber connectors (e.g., [29–33]). If fibers carry only strain energy associated with the axial deformation mode, or if fibers deform both in bending and axial modes but the connectors are rotating pins (do not transmit moments), the two thresholds are different. Transport percolation occurs at a smaller fraction of bonds present in the structure than stiffness percolation. This can be rationalized in terms of the coordination number which represents the number of bonds emerging from the given node. The critical coordination number that ensures the elimination of all floppy modes for central force networks can be determined using Maxwell's criterion (see [34] for a review). If fibers deform both in the bending and axial modes, the transport and stiffness percolation thresholds coincide, but the conductivity and stiffness problems do not belong to the same universality class [33]. The present discussion is qualitatively different from this body of literature. The mechanics of interlocked materials is controlled by the contacts between the component blocks and hence stiffness percolation in such cases is related

to the topology of the percolating cracks. The blocks forming the contacts are stiff, mechanically stable continua. Hence, this present problem is not immediately amenable to the random network case.

B. Comparison of modeling and experimental results

It is of interest to discuss the stress-strain response of samples with various f and to compare the behavior of structures with f above and below f_{c1}. For $f < f_{c1}$, the samples contain microcracks, but the response is linear elastic with effective stiffness predicted by the data in Fig. 3. For $f_{c1} < f < f_{c2}$, the response becomes nonlinear. The effective stiffness essentially vanishes at small strains. As the strain increases, the stress-strain curve asymptotes to a straight line of slope equal to the effective modulus reported in Fig. 3. This modulus is controlled by the stiffness of overhangs along the percolation path, while the deformation during the small strain regime is controlled by the gradual engagement of these overhangs. The nonlinearity originates from the distribution of gap sizes. Figure 5 shows two stress-strain curves corresponding to samples with $f = 0.63 < f_{c1}$ and $f = 0.75 > f_{c1}$. The vertical axis is normalized with E_{eff} (Fig. 3) and hence the asymptote at large strains has slope 1.

Such behavior is observed in other material systems close to the stiffness percolation threshold. An example is provided by random fiber networks, as discussed above. It has been shown that a floppy network can be rendered mechanically stable, with finite stiffness, if subjected to strain [35,36]. This is due to the preferential alignment of fibers which changes the architecture of the material.

Itacolumite is an example of material with topologically interlocked structure. As previously shown, the grains are separated by gaps which form a percolated network of channels [37]. The material of the grains (quartz) is brittle and has high modulus ($E_0 = 72$ GPa) under ambient conditions, but the rock is flexible and deforms under small loads (see Supplemental Material [18]). This behavior does not depend on the grain geometric irregularity [16,38]. Furthermore, the rock is sedimentary and has a quasilayered structure. This allows comparing the present 2D results with test results obtained with the 3D rock. We have tested samples of itacolumite originating from the North Carolina deposit in uniaxial tension and under strain rates of 10^{-3} s^{-1}. Samples were cut from the rock mass with the strata oriented in the loading direction. A thin section was prepared and observed with an optical microscope (Fig. 5 shows a view perpendicular to the strata). The width of the gaps between grains is approximately 3% of the grain size (which is 140 μm, as measured by the line intercept method) and is uniform across the sample. This indicates that the sample preserves mechanical stiffness due to the interlocking of the grains. Samples have a rectangular cross section of 10×5 mm, both dimensions being much larger than the grain size. The resulting stress-strain curve is shown in Fig. 5 (symbols). The ratio E_{eff}/E_0, with E_{eff} evaluated from the straight branch after the initial, small strain range, is approximately 10^{-3}. These structural and mechanical observations, along with similar results reported in the literature [17], indicate that itacolumite is a microcracked topologically interlocked material with stochastic microstructure, with a density of cracks larger than the transport percolation threshold, of the type discussed in this article.

IV. CONCLUSIONS

Increasing the crack density in randomly microcracked materials above the density corresponding to transport percolation leads to a topologically interlocked structure which preserves stiffness. This demonstrates that the transport and stiffness percolation thresholds are different even in two dimensions. The density of microcracks corresponding to stiffness percolation is estimated to be $f_{c2} = 0.78$ (compared to the transport percolation which occurs at $f_{c1} = 0.667$) and in the vicinity of the threshold the effective stiffness of the sample varies as $E_{\text{eff}}/E_0 \sim (f_{c2} - f)^{2.0 \pm 0.1}$. In the range of crack densities bounded by f_{c1} and f_{c2}, the effective material behavior is nonlinear. The initial part of the stress-strain curve exhibits stiffening, which is due to the gradual engagement of interlocks. At larger strains the stress-strain curves become linear. This behavior is analogous to that of itacolumite, a sandstone with high density of grain boundary cracks. This rock exhibits macroscopic flexibility highly unusual for a brittle material; see the Supplemental Material movie [18]. These findings provide a recipe for creating topologically interlocked materials with stochastic microstructure which can be used in a variety of applications, as discussed in the Introduction.
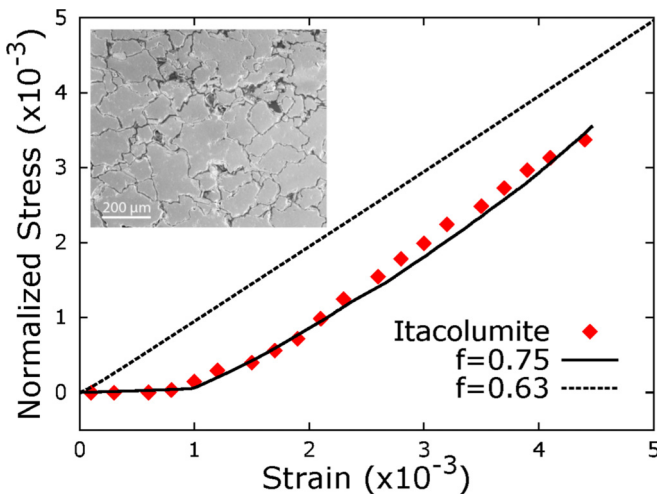

FIG. 5. Uniaxial tension stress-strain curves for 2D samples with $f = 0.75$ (continuous line) and 0.63 (dashed line) and for a 3D sample of itacolumite (symbols). The vertical axis is normalized with E_{eff} (Fig. 3) and, for the itacolumite, with the slope of the asymptote at larger strains.

[1] T. Mura, *Micromechanics of Defects in Solids* (Martinus Nijhoff, The Hague, Netherlands, 1982).

[2] H. P. Hsu and M. C. Huang, Phys. Rev. E **60**, 6361 (1999).

[3] A. M. Becker and R. M. Ziff, Phys. Rev. E **80**, 041101 (2009).

[4] Y. B. Yi and E. Tawerghi, Phys. Rev. E **79**, 041134 (2009).

[5] D. Krajcinovic, Eng. Fract. Mech. **57**, 227 (1997).

[6] D. Krajcinovic, K. Mallick, M. Batista, and D. Sumarac, Int. J. Solids Struct. **29**, 1837 (1992).

[7] A. V. Dyskin, Y. Estrin, A. J. Kanel-Belov, and E. Pasternak, Scripta Mater. **44**, 2689 (2001).

[8] Y. Estrin, A. V. Dyskin, and E. Pasternak, Mater. Sci. Eng., C **31**, 1189 (2011).

[9] J. D. Hiller, J. Miller, and H. Lipson, J. Microelectromech. Syst. **20**, 1089 (2011).

[10] S. Khandelwal, T. Siegmund, R. J. Cipra, and J. S. Bolton, J. Appl. Mech. **81**, 031011 (2014).

[11] A. V. Dyskin, Y. Estrin, E. Pasternak, H. C. Khor, and A. J. Kanel-Belov, Adv. Eng. Mater. **5**, 116 (2003).

[12] Y. Feng, T. Siegmund, E. Habtour, and J. Riddick, Int. J. Impact Eng. **75**, 140 (2015).

[13] M. Carlesso, R. Giacomelli, T. Krause, A. Molotnikov, D. Koch, S. Kroll, K. Tushtev, Y. Estrin, and K. Rezwan, J. Eur. Ceram. Soc. **33**, 2549 (2013).

[14] R. O. Ritchie, Nat. Mater. **10**, 817 (2011).

[15] K. Miszta, J. de Graaf, G. Bertoni, D. Dorfs, R. Brescia, S. Marras, L. Ceseracciu, R. Cingolani, R. van Roij, M. Dijkstra, and L. Manna, Nat. Mater. **10**, 872 (2011).

[16] H. K. Kerbey, Proc. Geol. Assoc. **122**, 16 (2011).

[17] M. B. Dusseault, Q. J. Eng. Geol. **13**, 119 (1980).

[18] See Supplemental Material at http://link.aps.org/supplemental/10.1103/PhysRevE.93.043005 for a movie showing the deformation of itacolumite, a rock exhibiting spectacular flexibility.

[19] T. Shimazu, M. Miura, N. Isu, T. Ogawa, K. Ota, H. Maeda, and E. H. Ishida, Mater. Sci. Eng., A **487**, 340 (2008).

[20] I. Sato, Y. Ichikawa, J. Sakanoue, M. Mizutani, N. Adachi, and T. Ota, J. Am. Ceram. Soc. **91**, 607 (2008).

[21] B. Berkowitz and R. P. Ewing, Surveys Geophys. **19**, 23 (1998).

[22] B. Budiansky and R. J. O'Connell, Int. J. Solids Struct. **12**, 81 (1976).

[23] S. Nemat-Nasser and M. Horii, *Micromechanics: Overall Properties of Heterogeneous Materials* (Elsevier, Amsterdam, 1999).

[24] M. Kachanov, Adv. Appl. Mech. **30**, 260 (1994).

[25] I. Jasiuk, J. Chen, and M. F. Thorpe, Appl. Mech. Rev. **47**, S18 (1994).

[26] D. Sornette, J. Phys. (Paris) **49**, 1365 (1988).

[27] D. Deptuck, J. P. Harrison, and P. Zawadzki, Phys. Rev. Lett **54**, 913 (1985).

[28] E. H. Saenger, O. S. Kruger, and S. A. Shapiro, Geophys. Prospecting **52**, 183 (2004).

[29] S. Feng and P. N. Sen, Phys. Rev. Lett. **52**, 216 (1984).

[30] K. Sieradzki and R. Li, Phys. Rev. Lett. **56**, 2509 (1986).

[31] A. R. Day, K. A. Snyder, E. J. Garboczi, and M. F. Thorpe, J. Mech. Phys. Solids **40**, 1031 (1992).

[32] Y. Kantor and I. Webman, Phys. Rev. Lett. **52** 1891 (1984).

[33] D. J. Jacobs and M. F. Thorpe, Phys. Rev. E **53**, 3682 (1996).

[34] R. C. Picu, Soft Matter **7**, 6768 (2011).

[35] M. F. Thorpe and Y. Cai, J. Non-Cryst. Solids **114**, 19 (1989).

[36] M. Wyart, H. Liang, A. Kabla, and L. Mahadevan, Phys. Rev. Lett. **101**, 215501 (2008).

[37] H. Suzuki and D. Shimizu, J. Geol. Soc. Jpn. **99**, 391 (1993).

[38] H. Suzuki, T. Yokoyama, and M. Nishihara, J. Geol. Soc. Jpn. **99**, 443 (1993).